# Heliyon

CrossMark

# Gene expression alterations in the medial prefrontal cortex and blood cells in a mouse model of depression during menopause

**Shigeo Miyata** [a,b,\*], **Masashi Kurachi** [c], **Noriko Sakurai** [a], **Yuchio Yanagawa** [b], **Yasuki Ishizaki** [c], **Masahiko Mikuni** [a], **Masato Fukuda** [a]

[a] *Department of Psychiatry and Neuroscience, Gunma University Graduate School of Medicine, Maebashi, Japan*

[b] *Department of Genetic and Behavioral Neuroscience, Gunma University Graduate School of Medicine, Maebashi, Japan*

[c] *Department of Molecular and Cellular Neurobiology, Gunma University Graduate School of Medicine, Maebashi, Japan*

\* Corresponding author at: Department of Psychiatry and Neuroscience, Gunma University Graduate School of Medicine, 3-39-22 Showa-machi, Maebashi, Gunma 371-8511, Japan.

E-mail address: s_miyata@gunma-u.ac.jp (S. Miyata).

## Abstract

**Aims:** The prevalence of major depressive disorder (MDD) is higher in women than in men, and this may be due to the decline in estrogen levels that occurs during the menopausal transition. We studied the biological alterations in the medial prefrontal cortex (mPFC), which is a region that is highly implicated in the neurobiology of MDD, and the blood cells (BCs) of ovariectomized (OVX) mice subjected to chronic mild stress (CMS), which represents a mouse model of depression during menopause.

**Main methods:** The mPFC and the BCs were obtained from the same individuals. Gene expression levels were analyzed by microarray. The data were used for the Ingenuity Pathway Analysis and the Gene Ontology analysis.

**Key findings:** The gene expression alterations (GEAs) induced by OVX were mainly associated with ribosomal and mitochondrial functions in both the mPFC

and the BCs. Rapamycin-insensitive companion of mTOR (RICTOR) was identified as a possible upstream regulator of the OVX-induced GEAs in both tissues. The CMS-induced GEAs were associated with retinoic acid receptor signaling, inflammatory cytokines and post-synaptic density in the mPFC, but not in the BCs.

**Significance:** OVX and CMS independently affect biological pathways in the mPFC, which is involved in the development of the depression-like phenotype. Because a subset of the OVX-induced GEAs in the mPFC also occurred in the BCs, the GEAs in the BCs might be a useful probe to predict biological pathways in the corresponding brain tissue under specific conditions such as OVX in females.

Keywords: Psychiatry, Neuroscience, Endocrinology

## 1. Introduction

Major depressive disorder (MDD) is a highly prevalent psychiatric disorder that is associated with physical impairment, medical comorbidity, and mortality worldwide (Sato and Yeh, 2013). A recent study measuring the global burden of disease with disability-adjusted life years suggested that a severe episode of MDD was a top contributor to disability among a variety of nonfatal consequences of disease and injury (Salomon et al., 2012). Biological, genetic, and environmental factors have been found to play crucial roles in the development of MDD (Levinson, 2006; Naismith et al., 2012; Nestler et al., 2002; Sato and Yeh, 2013); however, the exact pathogenesis and the underlying mechanisms that generate depressive symptoms remain largely unknown.

The prevalence of MDD is higher in women than in men, and this may be associated with the oscillations in and decline in estrogen levels that occur during the reproductive years and the menopausal transition (Deecher et al., 2008; Hunter, 1992). In addition, psychosocial stressors such as children leaving home, the death and illness of family members, the stresses of daily living, and health and the onset of chronic disease are known as inducible factors for MDD in menopausal women (Kaufert et al., 2008). In preclinical studies, female rodents with bilateral ovariectomies (OVXs) are frequently used as a model of menopause in women (Cho et al., 2004; Liu et al., 2004). In addition, previous reports, including ours, suggested that OVX rodents are vulnerable to stress and exhibit behavioral abnormalities similar to animal models of depression when subjected to chronic mild stress (CMS) (Lagunas et al., 2010; Miyata et al., 2016; Nakagawasai et al., 2009). Therefore, OVX rodents subjected to CMS are likely a reasonable animal model of depression during menopause.

The major aim of this study was to determine the gene expression patterns and their biological annotations in the medial prefrontal cortex (mPFC), which is a region

highly implicated in the neurobiology of MDD (Price and Drevets, 2012; Rive et al., 2013), in OVX mice compared to sham-operated mice with or without exposure to CMS. Next, we investigated the gene expression alterations (GEAs) and the GEA-associated biological annotations in the mPFC and blood cells (BCs) obtained from the same individuals, and we compared the GEAs and the biological annotations between the two tissues. The second aim of this study was to evaluate the possibility that the GEAs in BCs could potentially act as probes to monitor corresponding brain tissues because several studies have suggested potential molecules and biological pathways relevant to the neurobiology of MDD on the basis of GEA data from patients' BCs (Higuchi et al., 2011; Hori et al., 2016; Iga et al., 2005; Rocc et al., 2002).

## 2. Materials and methods

### 2.1. Animals

Female C57BL/6J mice (8 weeks of age) were purchased from Charles River Laboratories Japan, Inc. (Kanagawa, Japan). The mice were housed in groups of 6 per cage (16.5 cm × 27 cm × 12.5 (H) cm) and had free access to food and water. The animal room was maintained at $22 \pm 3$ °C with a 12-h light/dark cycle (lights on at 6:00 h, lights off at 18:00 h). The mice were acclimated to the laboratory environment for 1 week and were then ovariectomized bilaterally or underwent a sham operation under sodium pentobarbital (50 mg/kg, i.p.) anesthesia. All of the control mice used in this study were subjected to sham operation.

Two weeks after the OVX surgery, the CMS procedure was initiated. The mice were exposed to CMS for 6 weeks in accordance with our previous report (Miyata et al., 2016). Three stressors were used in this study (Table 1). For the first stressor, two of five diurnal stressors were delivered over a 1-h period in the morning and over a 2-h period in the evening, with a 2-h stress-free period between the two stressors. The five diurnal stressors included cage tilt (45°), small cage restriction (9.5 cm × 17 cm × 10.5 (H) cm), switching to the home-cage of another group, a soiled cage (50 ml of water in sawdust bedding), and odor (50% acetic acid). The

**Table 1.** Weekly schedule of the CMS protocol.

|  | Mon | Tue | Wed | Thu | Fri | Sat | Sun |
|---|---|---|---|---|---|---|---|
| 10:00–11:00 (1 h) | Small cage | Home-cage switching | Tilted cage | Odor | Small cage | Reverse light/dark | Reverse light/dark |
| 13:00–15:00 (2 h) | Odor | Soiled cage | Small cage | Home-cage switching | Tilted cage |  |  |
| 16:00–10:00 (overnight) | Difficult access to food | Overnight illumination | Tilted cage | Soiled cage | Reverse light/dark |  |  |

second stressor consisted of four nocturnal stressors applied between 16:00 h and 10:00 h, including one overnight period with difficult access to food, one overnight period with the lights on, one overnight period with a 45° cage tilt, and one overnight period in a soiled cage. For the third stressor, a reversed light/dark cycle was used from Friday evening to Monday morning. This procedure was scheduled over a 1-week period and was repeated six times. The non-stressed (NS) mice were handled weekly to clean the sawdust bedding.

This study was performed in accordance with the Guidelines for Animal Experimentation at Gunma University Graduate School of Medicine and was approved by the Gunma University Ethics Committee (Permit number: 12-006). Every effort was made to minimize the number of animals used and their suffering.

## 2.2. RNA extraction from blood cells and mPFC samples

One day after CMS cessation, mouse blood (300 µl) was collected under pentobarbital anesthesia (50 mg/kg, i.p.) via the vena cava. The blood was immediately heparinized and centrifuged (1,000 × $g$, 2 min). The total RNA in the pellet was extracted using the GeneJet Whole Blood RNA Purification Mini Kit (Thermo Fisher Scientific Inc.) according to the manufacturer's instructions.

Immediately after the blood was drawn, the mouse was decapitated, and the brain was removed. The decapitation was completed within 5 min of the anesthesia taking effect to minimize the effect of pentobarbital on gene expression. Coronal slices (1 mm thickness) were sectioned using a brain slicer, and the mPFC was dissected under a stereoscopic microscope (the dissected region on the brain map is illustrated in Supplementary Fig. 1). The dissected tissues were immersed in the RNA stabilization solution RNA*later* (Qiagen K.K., Tokyo, Japan) and stored until RNA extraction. Total RNA from the mPFC tissues was extracted using an RNeasy Micro Kit (Qiagen K.K.) according to the manufacturer's instructions.

Sampling of tissues was performed between 10:00 h and 16:00 h. The RNA quantity and quality were determined using a NanoDrop ND-1000 spectrophotometer (Thermo Fisher Scientific Inc.) and an Agilent Bioanalyzer (Agilent Technologies, Palo Alto, CA, USA) as recommended.

## 2.3. Microarray

Total RNA was amplified and labeled with Cyanine 3 (Cy3) using a one-color Agilent Low Input Quick Amp Labeling Kit (Agilent Technologies) according to the manufacturer's instructions. Briefly, 100 ng of total RNA was reverse-transcribed to obtain double-stranded cDNA using a poly dT-T7 promoter primer. The primer, template RNA, and quality-control transcripts of known concentrations and quality were first denatured at 65 °C for 10 min and then incubated for

2 h at 40 °C with 5 × first-strand buffer, 0.1 M dithiotreitol, 10 mM dNTP mix, and AffinityScript RNase Block Mix. The AffinityScript enzyme was then inactivated at 70 °C for 15 min. The cDNA products were used as templates for in vitro transcription to generate fluorescent cRNA. The cDNA products were mixed with a transcription master mix in the presence of T7 RNA polymerase and Cy3-labeled CTP and then incubated at 40 °C for 2 h. The labeled cRNAs were purified using Qiagen RNeasy mini spin columns and eluted using 30 μl of nuclease-free water. After the cRNA was amplified and labeled, the cRNA quantity and cyanine incorporation were determined using a NanoDrop ND-1000 spectrophotometer and an Agilent Bioanalyzer.

For each hybridization, 600 ng of Cy3-labeled cRNA was fragmented and hybridized at 65 °C for 17 h to an Agilent SurePrint G3 Mouse GE 8 × 60 K Microarray (Design ID: 028005). After washing, the microarrays were scanned using an Agilent DNA microarray scanner.

The intensity values of each scanned feature were quantified using Agilent feature extraction software version 10.7.3.1, which performs background subtractions. The normalization was performed using Agilent GeneSpring GX version 13.1.1 (per chip: normalization to the 75th percentile shift; per gene: none). The probes that were declared as "detected" in all the assayed samples and that displayed a raw intensity value above 50 in all samples were used for the following statistical analyses. Information concerning our data was submitted to the Gene Expression Omnibus with accession number GSE72262.

## 2.4. Ingenuity® Pathway Analysis

To identify the biological pathways, the data were analyzed using Ingenuity® Pathway Analysis (IPA®, QIAGEN Redwood City, www.qiagen.com/ingenuity). The probe IDs of GEAs with the expression values (logarithmic values of fold change) were uploaded; then, the pathway analysis was conducted. P-values lower than 0.05 for the Canonical Pathway Analysis and lower than 0.01 for the Upstream Regulator Analysis were defined as statistically significant. The IPA analysis was performed on Apr. 29, 2016.

## 2.5. Gene Ontology (GO) Analysis in DAVID

The biological annotations of GEAs were also assessed by GO analysis using DAVID bioinformatics resources version 6.8 (https://david.ncifcrf.gov/home.jsp). The list of genes declared as "present" in each tissue was used as the background for the analysis. Before supplying the dataset to DAVID, duplicate genes and probes without annotation or GenBank accession numbers were removed from the dataset. GO terms with a Bonferroni P-value less than 0.05 were considered statistically significant.

## 2.6. Statistics

For the microarray data, the factorial effects on the gene expression levels were determined by two-way ANOVA, and corrected *P*-values less than 0.05 (Benjamini-Hockberg false discovery rate <0.05) were considered significant. The number of theoretically matches of the GEAs between the two tissues was calculated using the following formula: (the total number of probes expressed in both tissues) × (the number of GEAs in the mPFC/the total number of probes expressed in the mPFC) × (the number of GEAs in the BCs/the total number of probes expressed in the BCs)/2. The odds ratios and 95% confidence intervals (CIs) between the actual and theoretical matching rates were calculated.

## 3. Results

### 3.1. GEAs in the mPFCs of the mice

We have previously reported that OVX mice subjected to the current CMS protocol show abnormalities in emotional behavior, including a prolonged duration of immobility in forced swimming tests, a decreased amount of time spent in the center of the field during open-field tests, and a decreased time duration in the open arms in elevated plus-maze tests without a change in locomotor activity (Miyata et al., 2016). In this study, we re-analyzed the same dataset and mice.

Four groups of mice (n = 6 in each group), sham + NS, OVX + NS, sham + CMS, and OVX + CMS, were used for the microarray analysis. In total, 24,496 probes were expressed in the mPFC. The two-way ANOVA revealed that the expression levels of 8,216 probes and 1,294 probes were significantly affected by OVX and CMS, respectively (Supplementary Tables 1 and 2). There was no interaction effect in the current analysis. We calculated the expression ratio (i.e., fold change) to identify the up-regulated or down-regulated probes among the 8,216 probes affected by OVX and the 1,294 probes affected by CMS. The results showed that OVX increased the expression levels of 5,453 probes and decreased the expression levels of 2,763 probes in the mPFC. CMS increased the expression levels of 797 probes and decreased the expression levels of 497 probes in the mPFC.

To determine the associated biological pathways, we performed an IPA and focused on the canonical pathways, specifically the pathways over-represented among the GEAs, and the upstream regulators, the potential molecules that caused the GEAs. Supplementary Table 3 shows the canonical pathways that were significantly associated with the OVX-induced GEAs in the mPFC. The 5 top-ranked pathways with the lowest *P*-values are shown in Fig. 1A and are as follows: EIF2 Signaling, Mitochondrial Dysfunction, Regulation of eIF4 and p70S6K Signaling, mTOR Signaling, and Oxidative Phosphorylation. The potential upstream regulators involved in the induction of the OVX-induced GEAs are
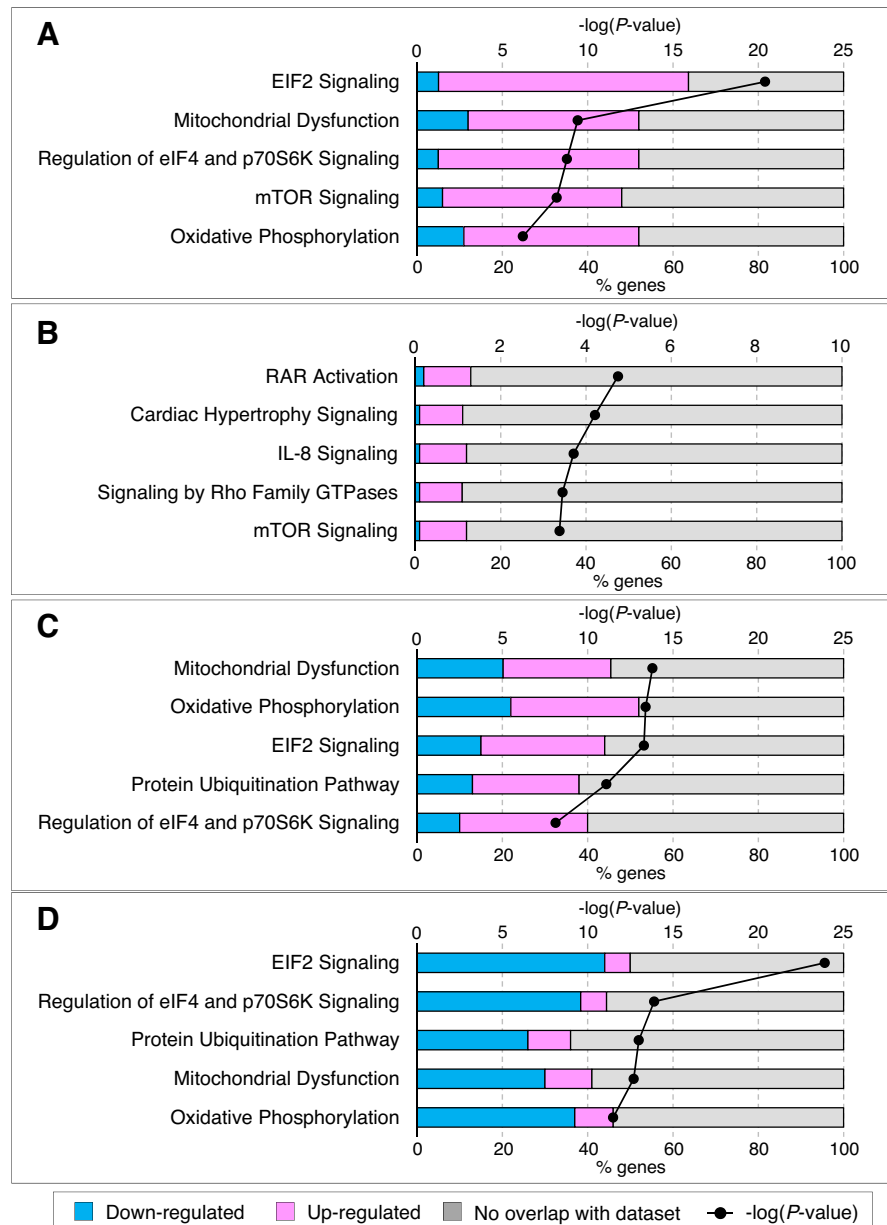
**Fig. 1.** The top-ranked canonical pathways associated with the GEAs. (A) The OVX-induced GEAs in the mPFC. (B) The CMS-induced GEAs in the mPFC. (C) The OVX-induced GEAs in the BCs. (D) The CMS-induced GEAs in the BCs. Other canonical pathways that were statistically significant are listed in Supplementary Tables 3, 5, 10 and 12.

shown in Supplementary Table 4. The top-ranked upstream regulator with the lowest *P*-value was rapamycin-insensitive companion of mTOR (RICTOR) (*P* < 4.29E-16); the predicted activation state was "inhibited". We also determined the canonical pathways and upstream regulators associated with the CMS-induced GEAs in the mPFC (Supplementary Tables 5 and 6). The 5 top-ranked pathways with the lowest *P*-values are shown in Fig. 1B and are as follows: RAR Activation, Cardiac

Hypertrophy Signaling, IL-8 Signaling, Signaling by Rho Family GTPases, and mTOR Signaling. The top-ranked upstream regulator with the lowest $P$-value associated with the CMS-induced GEAs was brain-derived neurotrophic factor (BDNF) ($P < 1.66E-07$); the predicted activation state was "activated".

We also determined the biological annotations of GEAs using GO analysis in DAVID. As shown in Table 2, the OVX-induced up-regulated genes in the mPFC are associated with ribosomal and mitochondrial functions, and the OVX-induced down-regulated genes in the mPFC are associated with olfactory function and keratin filament. The CMS-induced up-regulated genes in the mPFC are associated with the post-synaptic density, but there is no term over-represented by the CMS-induced down-regulated genes in the mPFC.

## 3.2. GEAs in the BCs of the mice

In total, 13,332 probes were expressed in the BCs. A two-way ANOVA revealed that the expression levels of 7,955 probes and 6,556 probes were significantly

**Table 2.** The GO terms associated with the GEAs in the mPFC.

| Category | Term | FE | P-values |
|---|---|---|---|
| <OVX-induced up-regulation> | | | |
| GOTERM_MF_DIRECT | GO:0003735~structural constituent of ribosome | 2.25 | 2.82E-23 |
| GOTERM_CC_DIRECT | **GO:0005840~ribosome** | 2.28 | 7.48E-22 |
| GOTERM_BP_DIRECT | **GO:0006412~translation** | 1.92 | 1.31E-19 |
| GOTERM_CC_DIRECT | GO:0022625~cytosolic large ribosomal subunit | 2.85 | 4.74E-14 |
| GOTERM_CC_DIRECT | GO:0005739~mitochondrion | 1.29 | 2.18E-11 |
| GOTERM_CC_DIRECT | **GO:0030529~intracellular ribonucleoprotein complex** | 1.68 | 2.69E-10 |
| GOTERM_MF_DIRECT | **GO:0044822~poly(A) RNA binding** | 1.27 | 2.11E-05 |
| GOTERM_CC_DIRECT | GO:0005743~mitochondrial inner membrane | 1.45 | 2.12E-04 |
| GOTERM_CC_DIRECT | GO:0015935~small ribosomal subunit | 2.66 | 1.97E-03 |
| GOTERM_CC_DIRECT | GO:0022627~cytosolic small ribosomal subunit | 2.22 | 5.33E-03 |
| <OVX-induced down-regulation> | | | |
| GOTERM_MF_DIRECT | **GO:0004984~olfactory receptor activity** | 7.23 | 3.96E-08 |
| GOTERM_BP_DIRECT | **GO:0007608~sensory perception of smell** | 5.13 | 5.55E-07 |
| GOTERM_CC_DIRECT | GO:0045095~keratin filament | 5.26 | 2.99E-04 |
| <CMS-induced up-regulation> | | | |
| GOTERM_CC_DIRECT | GO:0014069~postsynaptic density | 2.34 | 0.04 |
| <CMS-induced down-regulation> | | | |
| *None* | | | |

The GO terms were determined by DAVID (ver. 6.8) analysis. GO terms with a Bonferroni $P$-value less than 0.05 were considered statistically significant. GO terms shown in boldface indicate the overlap between the two tissues (see Table 3). FE: Fold enrichment.

affected by OVX and CMS, respectively (Supplementary Tables 7 and 8). Furthermore, 9 probes were significantly affected by the OVX × CMS interaction (Supplementary Table 9), although the effect was much smaller than the two main effects. We calculated the expression ratio to identify the up-regulated or down-regulated probes among the 7,955 OVX-induced probes and the 6,556CMS-induced probes. OVX increased the expression levels of 3,504 probes and decreased the expression levels of 4,451 probes in the BCs. CMS increased the expression levels of 2,509 probes and decreased the expression levels of 4,047 probes in the BCs.

Supplementary Table 10 shows the canonical pathways that were significantly associated with the OVX-induced GEAs in the BCs. The 5 top-ranked pathways with the lowest *P*-values are shown in Fig. 1C and are as follows: Mitochondrial Dysfunction, Oxidative Phosphorylation, EIF2 Signaling, Protein Ubiquitination Pathway, and Regulation of eIF4 and p70S6K Signaling. The potential upstream regulators involved in the induction of the OVX-induced GEAs are shown in Supplementary Table 11. The top-ranked upstream regulator with the lowest *P*-value was RICTOR ($P < 1.36E-36$); the predicted activation state was "inhibited". We also determined the canonical pathways and the upstream regulators associated with the CMS-induced GEAs in the BCs (Supplementary Tables 12 and 13). The 5 top-ranked pathways with the lowest *P*-values in each analysis are shown in Fig. 1D and are as follows: EIF2 Signaling, Regulation of eIF4 and p70S6K Signaling, Protein Ubiquitination Pathway, Mitochondrial Dysfunction, and Oxidative Phosphorylation. The top-ranked upstream regulator causing the CMS-induced GEAs in the BCs was RICTOR ($P < 9.79E-35$); the predictive activation state was "activated".

Using GO analysis, the OVX-induced up-regulated genes in the BCs are associated with transcriptional and translational functions, and the OVX-induced down-regulated genes in the BCs are associated with olfactory function, G-protein coupled receptor signaling pathways, plasma membrane, ion channels and transports (Table 3). The CMS-induced up-regulated genes in the BCs are associated with olfactory function and G-protein coupled receptor signaling pathways and are integral components of the plasma membrane. The CMS-induced down-regulated genes in the BCs are associated with transcriptional and translational functions (Table 3).

## 3.3. Comparison of GEAs between the mPFC and the BCs

GEAs in patients' BCs are of interest as a means to assess the molecules and pathways relevant to the pathogenesis of MDD, given that biopsy of the brain tissue is not feasible. Several studies have suggested potential molecules and biological pathways relevant to the neurobiology of MDD on the basis of GEA

**Table 3.** The GO terms associated with the GEAs in the BCs.

| Category | Term | FE | P-values |
|---|---|---|---|
| <OVX-induced up-regulation> | | | |
| GOTERM_MF_DIRECT | **GO:0044822~poly(A) RNA binding** | 1.46 | 6.18E-19 |
| GOTERM_MF_DIRECT | GO:0003723~RNA binding | 1.48 | 1.53E-10 |
| GOTERM_CC_DIRECT | GO:0005654~nucleoplasm | 1.29 | 3.05E-10 |
| GOTERM_CC_DIRECT | GO:0005634~nucleus | 1.14 | 6.16E-10 |
| GOTERM_CC_DIRECT | **GO:0030529~intracellular ribonucleoprotein complex** | 1.56 | 4.02E-07 |
| GOTERM_CC_DIRECT | GO:0016607~nuclear speck | 1.78 | 3.72E-06 |
| GOTERM_BP_DIRECT | GO:0006397~mRNA processing | 1.61 | 9.09E-06 |
| GOTERM_CC_DIRECT | GO:0005730~nucleolus | 1.33 | 6.41E-05 |
| GOTERM_MF_DIRECT | GO:0003676~nucleic acid binding | 1.33 | 3.32E-04 |
| GOTERM_BP_DIRECT | **GO:0006412~translation** | 1.48 | 3.36E-04 |
| GOTERM_CC_DIRECT | **GO:0005840~ribosome** | 1.57 | 5.19E-04 |
| GOTERM_CC_DIRECT | GO:0005681~spliceosomal complex | 1.73 | 7.37E-04 |
| GOTERM_BP_DIRECT | GO:0008380~RNA splicing | 1.57 | 2.69E-03 |
| GOTERM_CC_DIRECT | GO:0071013~catalytic step 2 spliceosome | 1.83 | 6.48E-03 |
| GOTERM_BP_DIRECT | GO:0006351~transcription, DNA-templated | 1.21 | 8.61E-03 |
| <OVX-induced down-regulation> | | | |
| GOTERM_MF_DIRECT | GO:0004930~G-protein coupled receptor activity | 2.01 | 8.25E-09 |
| GOTERM_BP_DIRECT | **GO:0007608~sensory perception of smell** | 2.50 | 1.02E-07 |
| GOTERM_BP_DIRECT | GO:0007186~G-protein coupled receptor signaling pathway | 1.78 | 7.64E-07 |
| GOTERM_MF_DIRECT | **GO:0004984~olfactory receptor activity** | 2.42 | 1.73E-06 |
| GOTERM_CC_DIRECT | GO:0005576~extracellular region | 1.48 | 4.72E-06 |
| GOTERM_CC_DIRECT | GO:0016021~integral component of membrane | 1.17 | 1.58E-04 |
| GOTERM_CC_DIRECT | GO:0005887~integral component of plasma membrane | 1.52 | 2.07E-04 |
| GOTERM_CC_DIRECT | GO:0045202~synapse | 1.69 | 3.09E-04 |
| GOTERM_CC_DIRECT | GO:0005886~plasma membrane | 1.18 | 1.09E-03 |
| GOTERM_MF_DIRECT | GO:0005216~ion channel activity | 2.33 | 1.14E-02 |
| GOTERM_BP_DIRECT | GO:0006811~ion transport | 1.61 | 1.28E-02 |
| GOTERM_MF_DIRECT | GO:0005249~voltage-gated potassium channel activity | 3.18 | 1.57E-02 |
| GOTERM_MF_DIRECT | GO:0005244~voltage-gated ion channel activity | 2.62 | 3.73E-02 |
| GOTERM_BP_DIRECT | GO:0034765~regulation of ion transmembrane transport | 2.68 | 4.26E-02 |
| <CMS-induced up-regulation> | | | |
| GOTERM_MF_DIRECT | GO:0004930~G-protein coupled receptor activity | 2.07 | 7.31E-04 |
| GOTERM_BP_DIRECT | GO:0007186~G-protein coupled receptor signaling pathway | 1.83 | 8.91E-03 |
| GOTERM_BP_DIRECT | GO:0007608~sensory perception of smell | 2.59 | 9.80E-03 |
| GOTERM_MF_DIRECT | GO:0004984~olfactory receptor activity | 2.48 | 2.60E-02 |
| GOTERM_CC_DIRECT | GO:0005887~integral component of plasma membrane | 1.59 | 3.96E-02 |

*(Continued)*

**Table 3**. (*Continued*)

| Category | Term | FE | P-values |
|---|---|---|---|
| <CMS-induced down-regulation> | | | |
| GOTERM_MF_DIRECT | GO:0044822~poly(A) RNA binding | 1.55 | 1.91E-32 |
| GOTERM_CC_DIRECT | GO:0005654~nucleoplasm | 1.37 | 7.41E-21 |
| GOTERM_CC_DIRECT | GO:0030529~intracellular ribonucleoprotein complex | 1.81 | 1.21E-19 |
| GOTERM_CC_DIRECT | GO:0005634~nucleus | 1.18 | 3.92E-19 |
| GOTERM_BP_DIRECT | GO:0006412~translation | 1.74 | 3.33E-16 |
| GOTERM_CC_DIRECT | GO:0005840~ribosome | 1.93 | 5.09E-16 |
| GOTERM_CC_DIRECT | GO:0005730~nucleolus | 1.51 | 8.01E-16 |
| GOTERM_MF_DIRECT | GO:0003723~RNA binding | 1.53 | 1.09E-15 |
| GOTERM_MF_DIRECT | GO:0003735~structural constituent of ribosome | 1.77 | 1.27E-11 |
| GOTERM_CC_DIRECT | GO:0016607~nuclear speck | 1.74 | 1.04E-06 |
| GOTERM_MF_DIRECT | GO:0000166~nucleotide binding | 1.23 | 5.63E-06 |
| GOTERM_MF_DIRECT | GO:0003676~nucleic acid binding | 1.34 | 6.27E-06 |
| GOTERM_BP_DIRECT | GO:0006351~transcription, DNA-templated | 1.25 | 7.73E-06 |
| GOTERM_CC_DIRECT | GO:0022625~cytosolic large ribosomal subunit | 1.98 | 1.29E-05 |
| GOTERM_MF_DIRECT | GO:0004386~helicase activity | 1.93 | 2.42E-05 |
| GOTERM_BP_DIRECT | GO:0006397~mRNA processing | 1.50 | 2.63E-04 |
| GOTERM_BP_DIRECT | GO:0016569~covalent chromatin modification | 1.53 | 6.65E-04 |
| GOTERM_CC_DIRECT | GO:0005681~spliceosomal complex | 1.66 | 9.81E-04 |
| GOTERM_MF_DIRECT | GO:0005524~ATP binding | 1.22 | 3.82E-03 |
| GOTERM_MF_DIRECT | GO:0004004~ATP-dependent RNA helicase activity | 2.16 | 4.16E-03 |
| GOTERM_CC_DIRECT | GO:0071013~catalytic step 2 spliceosome | 1.75 | 7.91E-03 |
| GOTERM_BP_DIRECT | GO:0006355~regulation of transcription, DNA-templated | 1.18 | 1.04E-02 |
| GOTERM_BP_DIRECT | GO:0006364~rRNA processing | 1.71 | 1.91E-02 |
| GOTERM_BP_DIRECT | GO:0008380~RNA splicing | 1.48 | 1.96E-02 |
| GOTERM_MF_DIRECT | GO:0003677~DNA binding | 1.19 | 2.90E-02 |
| GOTERM_BP_DIRECT | GO:0006260~DNA replication | 1.78 | 3.30E-02 |
| GOTERM_CC_DIRECT | GO:0022627~cytosolic small ribosomal subunit | 1.86 | 3.87E-02 |
| GOTERM_BP_DIRECT | GO:0042254~ribosome biogenesis | 1.83 | 4.01E-02 |
| GOTERM_CC_DIRECT | GO:0015030~Cajal body | 2.08 | 4.70E-02 |

The GO terms were determined by DAVID (ver. 6.8) analysis. GO terms with a Bonferroni P-value less than 0.05 were considered statistically significant. GO terms shown in boldface indicate the overlap between the two tissues (see Table 2). FE: Fold enrichment.

data from patients' BCs (Higuchi et al., 2011; Hori et al., 2016; Iga et al., 2005; Rocc et al., 2002); it is also noteworthy that these suggestions are based on published evidence that the genes (or proteins) of interest show alterations similar to those observed in the post-mortem brains of MDD patients. As the second aim of this study, we evaluated the concurrency of GEAs between the mPFC and the BCs in the mouse model.

We first cross-matched the probe names of the expressed genes and found a total of 11,210 probes (84.1% of the probes expressed in the BCs) that overlapped between the two tissues (Fig. 2A, Supplementary Table 14). For the 11,210 overlapping probes, the PCA scores were calculated and plotted (Fig. 2B). The PCA scores revealed that the first principal component (x-axis) explained 78.73%, the second principal component (y-axis) explained 7.54%, and the third principal component (z-axis) explained 4.72% of the gene expression. As shown, there was a distinct separation between the mPFC and the BCs.

**A**

**BCs**
(13,332 probes)

**mPFC**
(24,496 probes)

11,210
probes

**B**

Y-Axis

BC

mPFC

X-Axis

Z-Axis
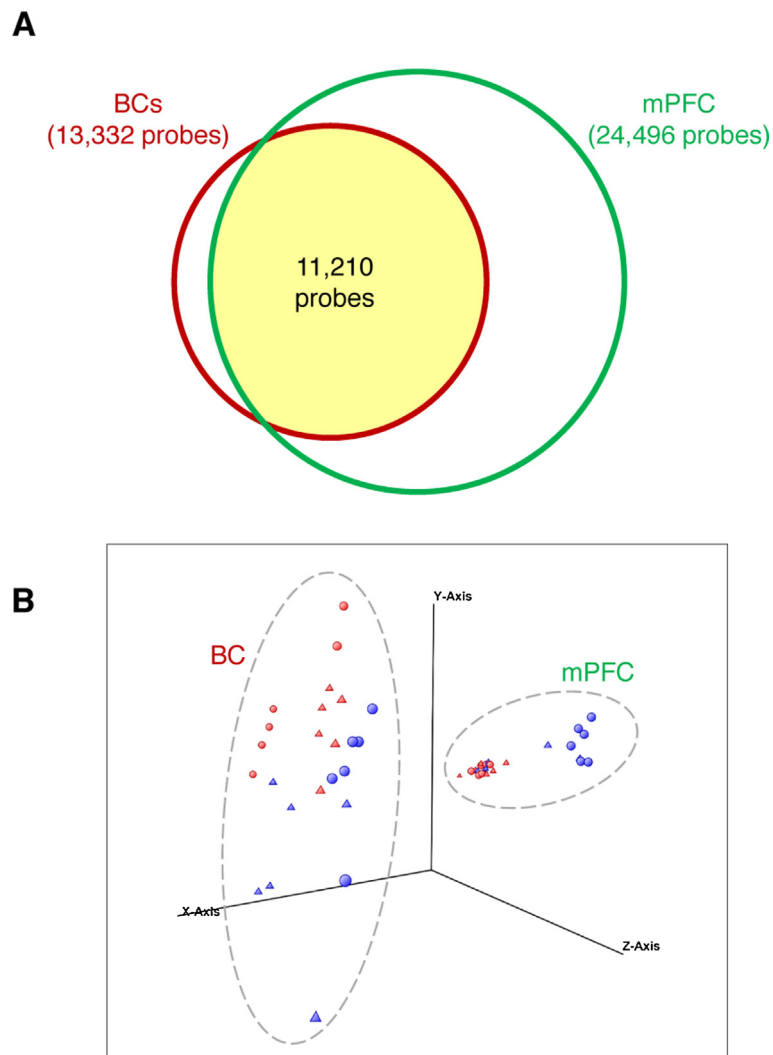
**Fig. 2.** Gene expression profiles in the mPFC and the BCs of the mice. (A) The number of genes expressed in the mPFC and the BCs is described in a Venn diagram. (B) The PCA scores of genes expressed in both the mPFC and the BCs. Each plot corresponds to the individual PCA score, is colored according to the operation (blue: sham-operated group, red: OVX group) and is shaped according to the stress treatment (circle: non-stressed group, triangle: CMS-treated group). The dashed circle indicates the tissues that the genes extracted.
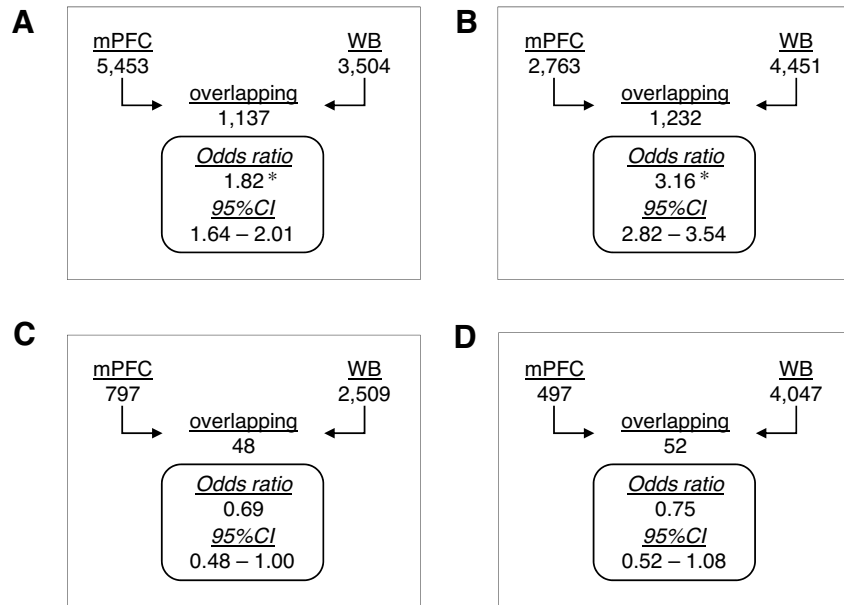
**Fig. 3.** Comparisons of the GEAs of the mPFC and BCs in the model mice. The OVX-induced up-regulated genes (A) and down-regulated genes (B) of the mPFC and the BCs were compared. The CMS-induced up-regulated genes (C) and down-regulated genes (D) of the mPFC and BCs were also compared. The significance of the actual matches compared with the theoretical matches was determined by calculating the odds ratios and 95% CIs, as shown in each panel of the figure. $*P < 0.001$ vs. the theoretical matching rates (Fisher's exact test).

We next compared the names of the GEA-associated probes of the two tissues. There was an overlap of 1,137 OVX-up-regulated probes between the two tissues (Fig. 3A). In addition, 1,232 OVX-down-regulated probes overlapped (Fig. 3B). Similarly, 48CMS-up-regulated probes overlapped (Fig. 3C), and 52 CMS-down-regulated probes overlapped (Fig. 3D).

It is possible that the matching of the probes was coincidental. To evaluate this possibility, the odds ratio and 95% CI were determined for the actual and theoretical matches. The theoretical number of matches of the OVX-induced up-regulated probes in the two tissues was 656. The odds ratio of the actual and theoretical matches for the OVX-induced up-regulated probes was 1.82 (95% CI: 1.64–2.01). Therefore, the number of actual matches of the OVX-induced up-regulated probes of the two tissues was statistically and significantly larger than the theoretical number of matches. Similarly, we compared the actual and theoretical matches for the OVX-induced down-regulated probes, the CMS-induced up-regulated probes, and the CMS-induced down-regulated probes between the two tissues; these results are summarized in Fig. 3A–D. Overall, the OVX-induced GEAs overlapped substantially between the mPFC and the WB in mice. However, the overlap between the GEAs induced by CMS in the two tissues was small, which indicated that the overlap between these GEAs might have been coincidental.

## 4. Discussion

In the mPFC, approximately 8,000 GEAs were observed as a response to OVX. The current IPA indicated that OVX affects EIF2 signaling, mitochondrial dysfunction, regulation of eIF4 and p70S6K signaling, mTOR signaling, and oxidative phosphorylation in the mPFC as the top-ranked canonical pathways. These pathways are associated with the regulation of protein biosynthesis and energy production. Given that the current GO analysis also indicated ribosomal and mitochondrial functions as over-represented terms in the OVX-induced up-regulated genes, it is likely that OVX affects the regulating pathways of protein biosynthesis and energy production in the mPFC. It is well established that eIFs (eukaryotic initiation factors) and p70S6K play critical roles in translational regulation. eIF2 is a GTP-binding protein that transports met-tRNA onto the 40S ribosome and promotes a new round of translation initiation by exchanging GDP for GTP (Kimball, 1999). eIF4 is involved in the recognition of the mRNA structure, delivery of RNA helicase and bridging of mRNA and ribosomes (Gingras et al., 1999). p70S6K is a serine/threonine protein kinase that phosphorylates the 40S ribosomal protein S6, which is involved in the translation of mRNAs (Ferrari and Thomas, 1994). The pathways of mitochondrial dysfunction and oxidative phosphorylation are related to the regulation of ATP production in mitochondria. Mechanistic (mammalian) target of rapamycin (mTOR) is a serine/threonine protein kinase that integrates various environmental cues, such as the signals from hormones, growth factors, nutrients, energy and stress, and regulates growth and homeostasis (Laplante and Sabatini, 2012). It has been reported that the expression levels of genes associated with protein biosynthesis and energy production are altered in the prefrontal cortex of the post-mortem brains of MDD patients (Klempan et al., 2009; Sibille et al., 2004). It has also been reported that OVX induces vulnerability to stress in female rodents (Lagunas et al., 2010; Miyata et al., 2016; Nakagawasai et al., 2009). Therefore, the dysregulated pathways associated with protein biosynthesis and energy production that were observed in the mPFC in the mice in the current study may be associated with the development of stress vulnerability. In the frontal cortex of ovariectomized rats, 17β-estradiol treatment regulated gene expression associated with transcriptional and metabolic functions (Sarvari et al., 2010a and 2010b). These biological pathways were also observed in the mPFC of the current OVX models. Estrogen stimulates estrogen receptors, thereby directly regulating transcription and translation in many cell types (Mueller et al., 1961; Hamilton, 1963; Bronson et al., 2010). This regulation is likely mediated by ribosome biogenesis (Ray et al., 2013). Therefore, estrogen deficiency induced by OVX may disrupt ribosomal function in many cell types. We assessed the upstream regulators causing the OVX-induced GEAs. Among them, RICTOR was found to be the top-ranked regulator associated with the production of OVX-induced GEAs in both

tissues. RICTOR is an essential component of target of rapamycin complex 2 (TORC2), in which it performs an important scaffolding function (Gaubitz et al., 2016; Wullschleger et al., 2005). The activity of TORC2 is regulated by lipid messengers, metabolic cues, membrane tension, and small GTPases (Chen et al., 2011; Dibble et al., 2009; Gan et al., 2011; Glidden et al., 2012; Saci et al., 2011). TORC2 phosphorylates AKT, SGK1, and PKCα and regulates their activities (Garcia-Martinez and Alessi, 2008, Guertin et al., 2006; Ikenoue et al., 2008; Sarbassov et al., 2005). In the central nervous system, RICTOR deletion affects the size, morphology, and function of neurons (Thomanetz et al., 2013). There is increasing evidence that the mTOR pathway plays a pivotal role in a rapid antidepressant action of ketamine (Abdallah et al., 2015; Abelaira et al., 2014; Carrier and Kabbaj, 2013; Miller et al., 2014). Although the biological effects of OVX on RICTOR activity remain unclear, the current IPA indicated that the induction of some of the GEAs by OVX was mediated by the inhibition of RICTOR in the mPFC. The current GO analysis indicates that the olfactory functions are associated with the OVX-induced down-regulated genes in the mPFC. Although the details of mechanisms remain unclear, ovarian hormones are necessary for both the production of and responsiveness to olfactory cues (Jechura and Lee, 2004).

Post-mortem studies have suggested that retinoic acid receptor (RAR) signaling and inflammatory cytokines (including interleukin-8) are involved in the neurobiology of mood disorders (Bremner and McCaffery, 2008; Qi et al., 2015; Shelton et al., 2011). In this study, approximately 1,000 GEAs were observed in the mPFC as a response to CMS. The CMS-induced GEAs were associated with the pathways of RAR activation and IL-8 signaling. We previously reported that OVX mice show no behavioral abnormalities but exhibit depression-like and anxiety-like behavior when subjected to CMS (Miyata et al., 2016). This observation is supported by a previous study showing that a milder form of CMS induces depression-like behavior in male mice of a stress-vulnerable strain (Balb/c) but not in male mice of a stress-resistant stain (C57BL/6J) (Uchida et al., 2011). Because the 5 top-ranked canonical pathways associated with the OVX-induced GEAs were largely different from those of the CMS-induced GEAs, OVX and CMS most likely had independent effects on the biological pathways in the mPFC. Therefore, it is likely that OVX plays a role in the induction of a vulnerability to stress, and CMS is a trigger for the development of a depressive-like phenotype in female mice. The post-synaptic density was over-represented as significant GO terms in the CMS-induced up-regulated genes. The functional change in the post-synaptic density might be involved in the behavioral phenotypes in CMS-treated mice. The current findings regarding biological annotations were compared with Erburu's study (Erburu et al., 2015) because the CMS protocol in the study was similar to ours, e.g., it used the same strain of mice

(C57BL/6J), the same duration of the CMS (6 weeks), and the same bioinformatics (IPA). However, the gender of mice in the studies differed. Several pathways, such as rho-mediated signals, were over-represented in both studies, but the other pathways were not overlapping. Therefore, gene expression alterations induced by CMS in the frontal cortex might differ between male and female mice.

The second aim of the current study was to evaluate the concurrency of GEAs in the mPFC and the BCs. In this experiment, we first compared the genes expressed in the BCs and the mPFC, and we found that 84% of the probes expressed in the BCs were also expressed in the mPFC. This finding is comparable to the results of a previous study assessing the concordance of gene expression in post-mortem human brains and peripheral BCs, which indicated a large overlap between the gene expression profiles of the brain tissues and the BCs (Liew et al., 2006). We also used PCA to investigate the expression levels of the genes in the mPFC and the BCs and found a distinct separation in the clusters in the PCA plots as a function of the tissues. Previous studies suggested that the expression levels of genes are weakly correlated between BCs and brain tissue (Bosker et al., 2012; Cai et al., 2010; Jasinska et al., 2009; Rollins et al., 2010). In accordance with previous studies, the current findings indicated that the patterns of intensity of gene expression were substantially different between the two tissues.

A two-way ANOVA revealed that OVX induced approximately 8,000 GEAs and CMS induced approximately 7,500 GEAs in the BCs. Comparisons of the top 5 canonical pathways associated with the OVX-induced GEAs and the CMS-induced GEAs (Fig. 3C and D) revealed a complete match between the two tissues, but the activation states were opposite. The associated pathways were mitochondrial dysfunction, oxidative phosphorylation, EIF2 signaling, the protein ubiquitination pathway, and regulation of eIF4 and p70S6K signaling. The protein ubiquitination system regulates the degradation of cellular proteins by proteasomes and autophagic systems that control the half-life and expression levels of proteins and the breakdown of misfolded and damaged proteins. The current findings indicate that OVX and CMS may elicit opposing effects on these pathways in BCs. The critical reason for this phenomenon remains unclear given that few studies have assessed the effects of OVX and CMS on the gene expression levels in blood cells, and the available information is currently minimal. However, Ivic et al. (2016) recently reported that the expression levels of gonadal steroid receptors, including estrogen receptor-β, were oppositely regulated by OVX and CMS in the hypothalamus. Therefore, it could be hypothesized that estrogen receptor-β expression levels in blood cells may also be oppositely regulated by OVX and CMS, and the opposite regulation of a subset of genes might be elicited.

In this study, we compared the patterns of the GEAs of the two tissues. Among the OVX-induced GEAs, the 1,137 up-regulated probes and the 1,232 down-regulated

probes overlapped between the two tissues, and these numbers were significantly larger than the theoretical number of matches. In addition, the major canonical pathways associated with the OVX-induced GEAs including their activation states were similar. These results indicate that the effects of OVX on the transcriptional systems are likely to be mediated by a common mechanism in both tissues. We assessed the upstream regulators causing the OVX-induced GEAs in the BCs. Among them, RICTOR was found to be the top-ranked regulator associated with the production of OVX-induced GEAs in the BCs. In thymocytes, RICTOR deletion impairs differentiation into T helper 1 (Th1) and 2 (Th2) cells (Lee et al., 2010). Although the biological effects of OVX on RICTOR activity remain unclear, the current IPA indicated that the induction of some of the GEAs by OVX was mediated by the inhibition of RICTOR in both the mPFC and BCs.

In contrast to the effect of OVX, the effects of CMS on the gene expression and biological pathways differed between the mPFC and BCs. The actual matching rates of the GEAs were not significantly different from the theoretical matching rates. The upstream regulators of the two tissues were also different, possibly because the major effect of CMS on the mPFC is mediated by alterations in neural activities such as BDNF signaling, but the effect of CMS on BCs may be mediated primarily by alterations in blood conditions, such as hormone levels and metabolic state.

However, we acknowledge a possibility that some of the differentially expressed genes and the pathways could be false positives. Therefore, further confirmation of any particular gene is needed before firm conclusions.

## 5. Conclusion

OVX and CMS independently affect biological functions, such as protein biosynthesis, energy production, RAR signaling and inflammatory cytokines, in the mPFC and lead to the depression-like phenotype observed in the mice in the current study. In addition, a subset of GEAs in the mPFC also occurred in the corresponding BCs under specific conditions such as OVX in females.

## Declarations

## Author contribution statement

Shigeo Miyata: Conceived and designed the experiments; performed the experiments; analyzed and interpreted the data; Wrote the paper.

Masashi Kurachi, Noriko Sakurai: Performed the experiments.

Yasuki Ishizaki: Analyzed and interpreted the data.

Yuchio Yanagawa, Masahiko Mikuni, Masato Fukuda: Wrote the paper.

## Competing interest statement

The authors declare no conflict of interest.

## Funding statement

## Additional Information

Supplementary content related to this article has been published online at http://dx.doi.org/10.1016/j.heliyon.2016.e00222

## Acknowledgments

## References

Abdallah, C.G., Sanacora, G., Duman, R.S., Krystal, J.H., 2015. Ketamine and rapid-acting antidepressants: a window into a new neurobiology for mood disorder therapeutics. Annu. Rev. Med. 66, 509–523.

Abelaira, H.M., Reus, G.Z., Neotti, M.V., Quevedo, J., 2014. The role of mTOR in depression and antidepressant responses. Life Sci. 101, 10–14.

Bosker, F.J., Gladkevich, A.V., Pietersen, C.Y., Kooi, K.A., Bakker, P.L., Gerbens, F., et al., 2012. Comparison of brain and blood gene expression in an animal model of negative symptoms in schizophrenia. Prog. Neuro-Psychopharmacol. Biol. Psychiatry 38, 142–148.

Bremner, J.D., McCaffery, P., 2008. The neurobiology of retinoic acid in affective disorders. Prog. Neuro-Psychopharmacol. Biol. Psychiatry 32, 315–331.

Bronson, M.W., Hillenmeyer, S., Park, R.W., Brodsky, A.S., 2010. Estrogen coordinates translation and transcription, revealing a role for NRSF in human breast cancer cells. Mol. Endocrinol. 24 (6), 1120–1135.

Cai, C., Langfelder, P., Fuller, T.F., Oldham, M.C., Luo, R., van den Berg, L.H., et al., 2010. Is human blood a good surrogate for brain tissue in transcriptional studies? BMC Genomics 11, 589.

Carrier, N., Kabbaj, M., 2013. Sex differences in the antidepressant-like effects of ketamine. Neuropharmacology 70, 27–34.

Chen, C.H., Shaikenov, T., Peterson, T.R., Aimbetov, R., Bissenbaev, A.K., Lee, S.W., et al., 2011. ER stress inhibits mTORC2 and Akt signaling through GSK-3beta-mediated phosphorylation of rictor. Sci. Signal. 4, ra10.

Cho, P., Schneider, G.B., Krizan, K., Keller, J.C., 2004. Examination of the bone-implant interface in experimentally induced osteoporotic bone. Implant Dent. 13, 79–87.

Deecher, D., Andree, T.H., Sloan, D., Schechter, L.E., 2008. From menarche to menopause: exploring the underlying biology of depression in women experiencing hormonal changes. Psychoneuroendocrinology 33, 3–17.

Dibble, C.C., Asara, J.M., Manning, B.D., 2009. Characterization of Rictor phosphorylation sites reveals direct regulation of mTOR complex 2 by S6K1. Mol. Cell. Biol. 29, 5657–5670.

Erburu, M., Cajaleon, L., Guruceaga, E., Venzala, E., Muñoz-Cobo, I., Beltrán, E., Puerta, E., Tordera, R.M., 2015. Chronic mild stress and imipramine treatment elicit opposite changes in behavior and in gene expression in the mouse prefrontal cortex. Pharmacol. Biochem. Behav. 135 (August), 227–236.

Ferrari, S., Thomas, G., 1994. S6 phosphorylation and the p70s6k/p85s6k. Crit. Rev. Biochem. Mol. Biol. 29, 385–413.

Gan, X., Wang, J., Su, B., Wu, D., 2011. Evidence for direct activation of mTORC2 kinase activity by phosphatidylinositol 3,4,5-trisphosphate. J. Biol. Chem. 286, 10998–11002.

Garcia-Martinez, J.M., Alessi, D.R., 2008. mTOR complex 2 (mTORC2) controls hydrophobic motif phosphorylation and activation of serum- and glucocorticoid-induced protein kinase 1 (SGK1). Biochem. J. 416, 375–385.

Gaubitz, C., Prouteau, M., Kusmider, B., Loewith, R., 2016. TORC2 structure and function. Trends Biochem. Sci.

Gingras, A.C., Raught, B., Sonenberg, N., 1999. eIF4 initiation factors: effectors of mRNA recruitment to ribosomes and regulators of translation. Annu. Rev. Biochem. 68, 913–963.

Glidden, E.J., Gray, L.G., Vemuru, S., Li, D., Harris, T.E., Mayo, M.W., 2012. Multiple site acetylation of Rictor stimulates mammalian target of rapamycin complex 2 (mTORC2)-dependent phosphorylation of Akt protein. J. Biol. Chem. 287, 581–588.

Guertin, D.A., Stevens, D.M., Thoreen, C.C., Burds, A.A., Kalaany, N.Y., Moffat, J., et al., 2006. Ablation in mice of the mTORC components raptor, rictor, or mLST8 reveals that mTORC2 is required for signaling to Akt-FOXO and PKCalpha, but not S6K1. Dev. Cell 11, 859–871.

Hamilton, T.H., 1963. Isotopic studies on estrogen-induced accelerations of ribonucleic acid and protein synthesis. Proc. Natl. Acad. Sci. U. S. A. 49, 373–379.

Higuchi, F., Uchida, S., Yamagata, H., Otsuki, K., Hobara, T., Abe, N., et al., 2011. State-dependent changes in the expression of DNA methyltransferases in mood disorder patients. J. Psychiatr. Res. 45, 1295–1300.

Hori, H., Sasayama, D., Teraishi, T., Yamamoto, N., Nakamura, S., Ota, M., et al., 2016. Blood-based gene expression signatures of medication-free outpatients with major depressive disorder: integrative genome-wide and candidate gene analyses. Sci. Rep. 6, 18776.

Hunter, M., 1992. The south-east England longitudinal study of the climacteric and postmenopause. Maturitas 14, 117–126.

Iga, J., Ueno, S., Yamauchi, K., Motoki, I., Tayoshi, S., Ohta, K., et al., 2005. Serotonin transporter mRNA expression in peripheral leukocytes of patients with major depression before and after treatment with paroxetine. Neurosci. Lett. 389, 12–16.

Ikenoue, T., Inoki, K., Yang, Q., Zhou, X., Guan, K.L., 2008. Essential function of TORC2 in PKC and Akt turn motif phosphorylation, maturation and signalling. EMBO J. 27, 1919–1931.

Ivic, V., Blazetic, S., Labak, I., Balog, M., Vondrak, L., Blazekovic, R., Vari, S.G., Heffer, M., 2016. Ovariectomy and chronic stress lead toward leptin resistance in the satiety centers and insulin resistance in the hippocampus of Sprague-Dawley rats. Croat. Med. J. 57 (April (2)), 194–206.

Jasinska, A.J., Service, S., Choi, O.W., DeYoung, J., Grujic, O., Kong, S.Y., et al., 2009. Identification of brain transcriptional variation reproduced in peripheral blood: an approach for mapping brain expression traits. Hum. Mol. Genet. 18, 4415–4427.

Jechura, T.J., Lee, T.M., 2004. Ovarian hormones influence olfactory cue effects on reentrainment in the diurnal rodent, Octodon degus. Horm. Behav. 46 (September (3)), 349–355.

Kaufert, P.A., Gilbert, P., Tate, R., 2008. The Manitoba Project: a re-examination of the link between menopause and depression. Maturitas 61, 54–66.

Kimball, S.R., 1999. Eukaryotic initiation factor eIF2. Int. J. Biochem. Cell Biol. 31, 25–29.

Klempan, T.A., Sequeira, A., Canetti, L., Lalovic, A., Ernst, C., ffrench-Mullen, J., et al., 2009. Altered expression of genes involved in ATP biosynthesis and GABAergic neurotransmission in the ventral prefrontal cortex of suicides with and without major depression. Mol. Psychiatry 14, 175–189.

Lagunas, N., Calmarza-Font, I., Diz-Chaves, Y., Garcia-Segura, L.M., 2010. Long-term ovariectomy enhances anxiety and depressive-like behaviors in mice submitted to chronic unpredictable stress. Horm. Behav. 58, 786–791.

Laplante, M., Sabatini, D.M., 2012. mTOR signaling in growth control and disease. Cell 149, 274–293.

Lee, K., Gudapati, P., Dragovic, S., Spencer, C., Joyce, S., Killeen, N., et al., 2010. Mammalian target of rapamycin protein complex 2 regulates differentiation of Th1 and Th2 cell subsets via distinct signaling pathways. Immunity 32, 743–753.

Levinson, D.F., 2006. The genetics of depression: a review. Biol. Psychiatry 60, 84–92.

Liew, C.C., Ma, J., Tang, H.C., Zheng, R., Dempsey, A.A., 2006. The peripheral blood transcriptome dynamically reflects system wide biology: a potential diagnostic tool. J. Lab. Clin. Med. 147, 126–132.

Liu, M.L., Xu, X., Rang, W.Q., Li, Y.J., Song, H.P., 2004. Influence of ovariectomy and 17beta-estradiol treatment on insulin sensitivity, lipid metabolism and post-ischemic cardiac function. Int. J. Cardiol. 97, 485–493.

Miller, O.H., Yang, L., Wang, C.C., Hargroder, E.A., Zhang, Y., Delpire, E., et al., 2014. GluN2B-containing NMDA receptors regulate depression-like behavior and are critical for the rapid antidepressant actions of ketamine. eLife 3, e03581.

Miyata, S., Kurachi, M., Okano, Y., Sakurai, N., Kobayashi, A., Harada, K., et al., 2016. Blood transcriptomic markers in patients with late-onset major depressive disorder. PLoS One 11, e0150262.

Mueller, G.C., Gorski, J., Aizawa, Y., 1961. The role of protein synthesis in early estrogen action. Proc. Natl. Acad. Sci. U. S. A. 47, 164–169.

Naismith, S.L., Norrie, L.M., Mowszowski, L., Hickie, I.B., 2012. The neurobiology of depression in later-life: clinical, neuropsychological, neuroimaging and pathophysiological features. Prog. Neurobiol. 98, 99–143.

Nakagawasai, O., Oba, A., Sato, A., Arai, Y., Mitazaki, S., Onogi, H., et al., 2009. Subchronic stress-induced depressive behavior in ovariectomized mice. Life Sci. 84, 512–516.

Nestler, E.J., Barrot, M., DiLeone, R.J., Eisch, A.J., Gold, S.J., Monteggia, L.M., 2002. Neurobiology of depression. Neuron 34, 13–25.

Price, J.L., Drevets, W.C., 2012. Neural circuits underlying the pathophysiology of mood disorders. Trends Cogn. Sci. 16, 61–71.

Qi, X.R., Zhao, J., Liu, J., Fang, H., Swaab, D.F., Zhou, J.N., 2015. Abnormal retinoid and TrkB signaling in the prefrontal cortex in mood disorder. Cereb. Cortex (New York, NY: 1991) 25, 75–83.

Ray, S., Johnston, R., Campbell, D.C., Nugent, S., McDade, S.S., Waugh, D., et al., 2013. Androgens and estrogens stimulate ribosome biogenesis in prostate and breast cancer cells in receptor dependent manner. Gene 526 (1), 46–53.

Rive, M.M., van Rooijen, G., Veltman, D.J., Phillips, M.L., Schene, A.H., Ruhe, H.G., 2013. Neural correlates of dysfunctional emotion regulation in major depressive disorder: a systematic review of neuroimaging studies. Neurosci. Biobehav. Rev. 37, 2529–2553.

Rocc, P., De Leo, C., Eva, C., Marchiaro, L., Milani, A.M., Musso, R., et al., 2002. Decrease of the D4 dopamine receptor messenger RNA expression in lymphocytes from patients with major depression. Prog. Neuro-Psychopharmacol. Biol. Psychiatry 26, 1155–1160.

Rollins, B., Martin, M.V., Morgan, L., Vawter, M.P., 2010. Analysis of whole genome biomarker expression in blood and brain. Am. J Med. Genet. B Neuropsychiatr. Genet. 153b, 919–936.

Saci, A., Cantley, L.C., Carpenter, C.L., 2011. Rac1 regulates the activity of mTORC1 and mTORC2 and controls cellular size. Mol. Cell 42, 50–61.

Salomon, J.A., Vos, T., Hogan, D.R., Gagnon, M., Naghavi, M., Mokdad, A., et al., 2012. Common values in assessing health outcomes from disease and injury: disability weights measurement study for the Global Burden of Disease Study 2010. Lancet 380, 2129–2143.

Sarbassov, D.D., Guertin, D.A., Ali, S.M., Sabatini, D.M., 2005. Phosphorylation and regulation of Akt/PKB by the rictor-mTOR comple. Science (New York, NY) 307, 1098–1101.

Sato, S., Yeh, T.L., 2013. Challenges in treating patients with major depressive disorder: the impact of biological and social factors. CNS Drugs 27 (Suppl. 1), S5–10.

Shelton, R.C., Claiborne, J., Sidoryk-Wegrzynowicz, M., Reddy, R., Aschner, M., Lewis, D.A., et al., 2011. Altered expression of genes involved in inflammation and apoptosis in frontal cortex in major depression. Mol. Psychiatry 16, 751–762.

Sibille, E., Arango, V., Galfalvy, H.C., Pavlidis, P., Erraji-Benchekroun, L., Ellis, S.P., et al., 2004. Gene expression profiling of depression and suicide in human prefrontal cortex. Neuropsychopharmacology 29, 351–361.

Thomanetz, V., Angliker, N., Cloetta, D., Lustenberger, R.M., Schweighauser, M., Oliveri, F., et al., 2013. Ablation of the mTORC2 component rictor in brain or Purkinje cells affects size and neuron morphology. J. Cell Biol. 201, 293–308.

Uchida, S., Hara, K., Kobayashi, A., Otsuki, K., Yamagata, H., Hobara, T., et al., 2011. Epigenetic status of Gdnf in the ventral striatum determines susceptibility and adaptation to daily stressful events. Neuron 69, 359–372.

Wullschleger, S., Loewith, R., Oppliger, W., Hall, M.N., 2005. Molecular organization of target of rapamycin complex 2. J. Biol. Chem. 280, 30697–30704.